INTERNATIONAL JOURNAL FOR NUMERICAL METHODS IN FLUIDS, VOL. 13, 321–340 (1991)

PREDICTION OF FLOW OVER HELICALLY RIBBED SURFACES

F. S. HENRY and M. W. COLLINS

Thermo-Fluids Engineering Research Centre, City University, Northampton Square, London EC1V 0HB, U.K.

SUMMARY

Fully developed, steady flow through an annulus with a multistart, helical-ribbed inner cylinder is numerically predicted and compared with available data. To facilitate comparison, the transverse-ribbed case is included. It is predicted that substantial differences exist between turbulent flow over helical ribs and that over transverse ribs. The predictions clarify the experimental finding that helical-ribbed cylinders can be expected to have better pressure drop and heat transfer characteristics than transverse-ribbed cylinders. For this work the AERE Harwell code FLOW3D Release 2 was used.

KEY WORDS Swirling flow Helically ribbed surfaces Nuclear fuel

1. INTRODUCTION

Flow over artificially roughened surfaces has been the subject of much study primarily because of the enhanced rates of heat transfer achievable from such surfaces. The roughened elements are commonly small ribs of square cross-section that are placed periodically and at right angles to the mean flow direction. The price paid for the higher heat transfer rates is an increase in pressure drop. There is also the possibility of 'hot spots' on the roughened surfaces if the elements cause the flow to separate.

Flow over surfaces with transverse ribs has been the subject of several experimental investigations. Most researchers have studied the flow over transverse-ribbed plane surfaces. Lawn's[1] data are probably the most extensive. Numerical predictions of these flows are less common. Wilkes and Firth[2] simulated some of Lawn's results for plane surfaces using the k–ε model. However, to the best of the authors' knowledge, no calculations for the annular case have been published.

Pirie[3] made a series of measurements of pressure drop and heat transfer in the flow through annuli with inner cylinders having multistart, helical ribs. Pirie's data showed that helical-ribbed surfaces have superior pressure drop and heat transfer characteristics when compared to surfaces with transverse ribs. However, to date, no measurements have been made of the details of the flow in the inter-rib channel, and hence the question of flow separation remains unanswered.

This paper describes the initial phase of a detailed numerical study of heat transfer from helical-ribbed cylinders in the context of the Advanced Gas-cooled Reactor fuel element. Specifically, this paper deals with the calculation of the steady, turbulent, fully developed flow field. For purposes of comparison, the transverse-ribbed case was also predicted.

0271–2091/91/130321–20$10.00

Received January 1990

2. NUMERICAL SOLUTION

The governing equations were solved using FLOW3D, which is a general, three-dimensional, flow-modelling code developed by AERE Harwell. FLOW3D uses a control volume approach and the current version (Release 2) allows the use of non-orthogonal body-fitted co-ordinates on a non-staggered grid. Body-fitted co-ordinates were necessary for the flow geometry under consideration. The code's standard k–ε model was employed together with wall functions at the solid boundaries. Details of the development of FLOW3D with body-fitted co-ordinates have been given by Burns *et al.*[4] and general details of FLOW3D by Jones *et al.*[5] The programme was run on the Cray 2 at Harwell using the IBM front-end.

3. FLOW DETAILS AND GRIDDING SYSTEMS

3.1. Geometrical and other flow details

Schematic diagrams of transverse- and helical-ribbed cylinders are given in Figure 1. Details of the five ribbed geometries considered are given in Table I. As can be seen, the rib (helix) angle is defined such that the transverse case has a value of 0°. In all cases the inner cylinder root diameter D_1 was taken to be 39·44 mm, the rib height e to be 1·13 mm, the rib pitch to be 7·29 mm and the inner diameter of the outer cylinder, D_2, to be 98·09 mm. The rib widths were chosen so that all geometries had the same value (0·8609 mm) in the axial direction and hence the same inter-rib

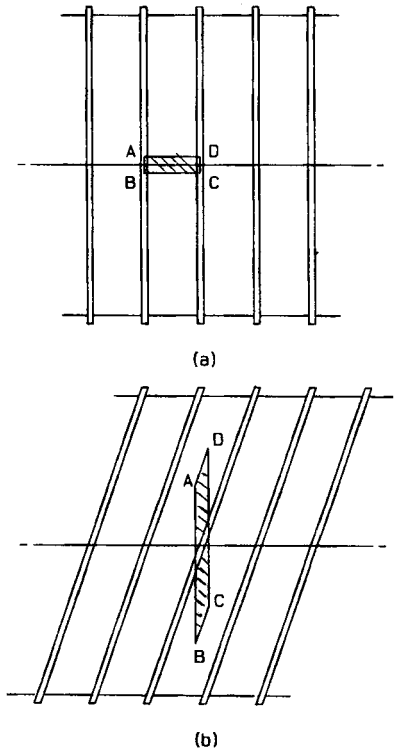

Figure 1. Schematic diagrams of ribbed surfaces

Table I. Flow channel geometry

Case	1	2	3	4	5
Number of starts	—	4	6	12	30
Rib angle (deg)	0	12·887	18·941	34·464	59·767
Rib width at mid-height (mm)	0·8609	0·8416	0·8153	0·7100	0·4335

Table II. Flow and fluid characteristics

Mass flow rate ($kg\,s^{-1}$)	0·45
Density ρ ($kg\,m^{-3}$)	1·15
Viscosity μ ($kg\,m^{-1}\,s^{-1}$)	$1{\cdot}96 \times 10^{-5}$
$Re = \rho(D_2 - D_1)U_m/\mu$	$2{\cdot}13 \times 10^5$

channel width in that direction. Further, the rib widths were chosen so that the 34° case matched that used by Pirie.[6] The smooth-walled annuli were assumed to have inner diameters of 39·44 mm and outer diameters of 98·09 mm.

To reduce the computational effort to a minimum, all flows were assumed to be incompressible and fully developed. It was further assumed that the density and molecular viscosity were not functions of temperature. The flow Reynolds number was chosen to match that used by Pirie.[6] Mass flow rate and fluid properties are given in Table II. In all cases the mass flow rate and density were kept constant at the values given in Table II. When required, the Reynolds number was changed by adjusting the viscosity.

3.2. Boundary conditions and grids for flow calculations

In the transverse-ribbed case the assumption of fully developed flow required the velocity field to be periodic in the axial direction. Note that the axial momentum equation was made periodic by defining a modified pressure field. The required modification is discussed in Section 4.1. The assumption of fully developed flow meant that it was necessary to model only one rib pitch. The solution domain for the transverse case is shown schematically in Figure 1(a) as the hatched area ABCD. The lines AB and CD denote planes of periodicity.

FLOW3D treats all flows as three-dimensional and requires dummy nodes at either end of all co-ordinate directions to implement boundary conditions. Consequently, the minimum number of control volumes in any one direction is three. For example, in the case of axisymmetric flows (as is the flow over transverse ribs) the grid has only one active node in the angular direction, but dummy nodes are required either side to satisfy the symmetry boundary conditions. The total number of control volumes (active and dummy) used in the transverse-ribbed case was $16 \times 24 \times 3$.

In the helical-ribbed case it was necessary to use a non-orthogonal grid. The solution domain for this case is shown schematically as the hatched area ABCD in Figure 1(b) and a sample grid is shown in Figure 2. In this case the assumption of fully developed flow meant that the flow was periodic in both the axial and angular directions. This double periodicity meant that it was necessary to model only the flow in the angular segment shown in Figure 2. The segment is bounded by planes of periodicity in the angular direction. These planes are shown schematically as lines AD and BC in Figure 1(b). Only one active control volume was necessary in the flow direction in this case, because the nature of the fully developed flow over the helical ribs is such

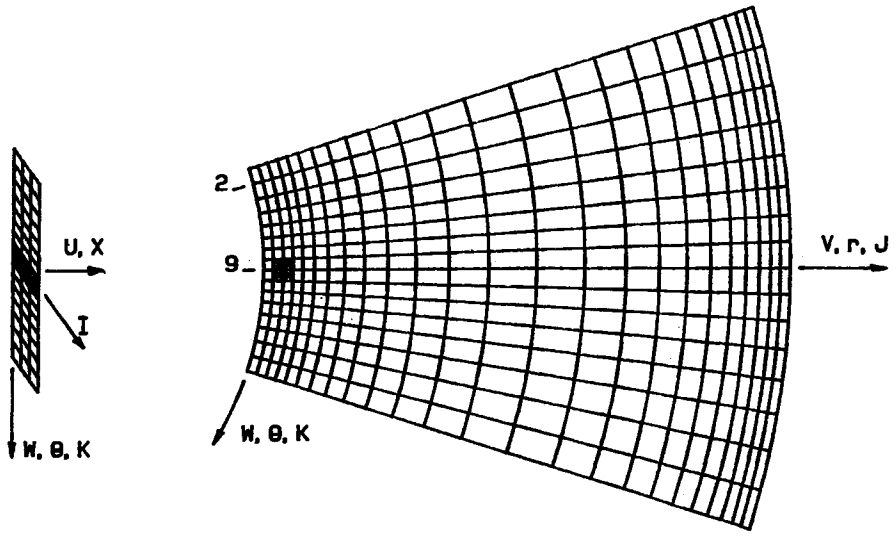

Figure 2. Grid slices for helical-ribbed case

that all flow quantities, except pressure, are constant for constant radial position in planes parallel to the ribs, i.e. in the direction denoted as I in Figure 2. Fully developed flow was generated by invoking periodic boundary conditions in the I-direction. Unless otherwise stated, all helical-ribbed predictions were generated on $3 \times 24 \times 16$ grids similar to that shown in Figure 2.

In order to ensure that all predictions were of comparable accuracy, the transverse grid was made geometrically similar to the helical grids. That is, the grids in the radial direction were identical and the same number of control volumes was used in the axial direction of the transverse grid as was used in the angular direction of the helical grids. Also, each active control volume in the axial direction of the transverse grid was made to correspond to an active control volume in the angular direction of the helical grids.

The correspondence between the two grids shown schematically in Figure 1 may not be immediately obvious. However, owing to the double periodicity of the helical flow, positions in the angular direction correspond identically to positions in the axial direction. That is, moving away from the rib in the angular direction at a constant axial position corresponds to moving away from the rib in the axial direction at a constant angular position. Hence, while the rib is in a different position in the helical grid to that in the transverse grid, individual control volumes in one grid correspond exactly to individual control volume in the other grid. Note that the plots of the change of various parameters in the helical flows with axial distance, discussed in Section 4, were constructed using this spatial correspondence.

The number of control volumes used to resolve the rib was limited by the need for the first computational point to be above the viscous sublayer. In fact, only two control volumes could be used over the rib height and a similar number across the rib width at the design Reynolds number ($2{\cdot}13 \times 10^5$). To reduce the total number of control volumes, the grid was expanded away from all solid surfaces.

4. PREDICTIONS

4.1. Smooth-walled annulus

Initial calculations were carried out for the flow through a smooth-walled annulus. These calculations were used primarily in the development and testing of the procedure to simulate fully developed, periodic flow with a fixed, known, mass flow rate. Fully developed flow was modelled by invoking the periodic boundary condition option in the axial (x-) direction. The axial momentum equation was made periodic by defining a periodic pseudo-pressure P^* such that

$$P^* = P + \Delta P x / l. \tag{1}$$

For fully developed flow over ribbed cylinders the pressure drop ΔP is the overall pressure drop per rib pitch; hence in this case l represents the rib pitch. In the case of smooth cylinders $\Delta P/l$ is simply the pressure drop per unit length. The pressure term in the axial momentum equation can be written as

$$-\frac{\partial P}{\partial x} = -\frac{\partial P^*}{\partial x} + \frac{\Delta P}{l}. \tag{2}$$

The pressure drop per unit length, $\Delta P/l$, is included as a source term in the axial momentum equation. The resulting equation is then periodic in both velocity and pseudo-pressure.

In FLOW3D all modifications to source terms are carried out in a user-defined routine called USRSRC. The original version of this routine was written such that, starting from any reasonable guess, the pressure drop was adjusted each iteration by a factor proportional to the ratio of the desired mass flow to the current mass flow. This resulted in the pressure drop being reduced if the current mass flow was too high and increased if the mass flow was too low. While this procedure eventually produced a converged solution, the predicted value of pressure drop oscillated for some considerable time. It was found that this oscillation could be greatly reduced with a minor modification to the original procedure. This entailed keeping a running average of the source pressure drop and reinitializing the current value with the average every 50 iterations. An unexpected bonus to this modification was that the axial momentum residual, used as a test of convergence, was reduced by several orders of magnitude.

Unfortunately, data of sufficient detail for the variation of the various flow parameters could not be found for turbulent flow in a smooth annulus. However, friction factor predictions could be compared with a number of experimental data. For instance, Lawn and Elliot[7] measured pressure drops for the fully developed flow of air in smooth annuli of various radius ratios. They found that, except for very small values of radius ratio, the friction factor was independent of radius ratio and, up to a Reynolds number of 10^5, the data were well matched by a line that lay 5% above the Blasius line for smooth pipe flow, i.e. the best fit line could be given as

$$f = 0{\cdot}079C(Re), \tag{3}$$

where $C = 1{\cdot}05$.

Estimates using the above correlation are compared with predictions in Table III. It can be seen that values estimated from Lawn and Elliot's correlation are well matched by the model. For Reynolds numbers below 10^5 the predictions and correlation values are within 1% of each other. As expected, at the highest Reynolds number considered the model's prediction is higher (3%) than the correlation values. Hence it can be concluded that FLOW3D can accurately predict the pressure drop in turbulent smooth annular flow.

Included in Table III are friction factor predictions for various grids for the lowest and highest Reynolds numbers. JV is the number of control volumes, of equal size, across the channel. It can

Table III. Theoretical and predicted friction factors for turbulent flow in a smooth annulus. All but last prediction produced using k–ε turbulence model. Last entry produced using full Reynolds stress (RS) model

							Friction factor	
Re	*JV*	$\Delta P/l$	τ_{w1}	τ_{w2}	y_1^+	y_2^+	Pred.	Exp.
$3{\cdot}00\times10^4$	24	949·5	−15·29	13·37	18·6	17·1	0·00630	0·00630
	36	962·6	−15·44	13·58	12·4	11·5	0·00639	
	48	1114·0	−17·50	15·86	9·9	9·3	0·00739	
$6{\cdot}00\times10^4$	24	793·3	−12·73	11·19	34·0	31·2	0·00526	0·00530
$1{\cdot}00\times10^5$	24	704·2	−11·27	9·95	53·5	49·1	0·00467	0·00466
$2{\cdot}13\times10^5$	24	599·5	−9·56	8·48	104·8	96·7	0·00398	0·00386
	36	597·9	−9·48	8·48	69·3	64·6	0·00397	
	48	597·7	−9·46	8·49	51·8	48·6	0·00396	
RS	24	865·6	−10·09	9·28	114·4	107·5	0·00574	

be seen that the predictions at the higher Reynolds number are little affected by the grid refinement. This is because in all three grids the near-wall boundary point is well outside the viscous sublayer. However, in the case of the lower-Reynolds-number predictions it can be seen that the friction factor is overpredicted by approximately 17% when the near-wall boundary point is forced into the viscous sublayer. The above illustrates the constraints placed upon grid refinement when wall functions are employed.

That the solution can be influenced by the position of the near-wall boundary point is not an unexpected result. Henry and Reynolds[8] have shown analytically that for plane Couette flow the point at which the model equations are matched to the near-wall boundary conditions is an important parameter of the solution.

4.2. Smooth-walled annulus with inner cylinder rotating

Bradshaw[9] showed that models based on the eddy viscosity concept cannot be expected to predict accurately flows with significant streamline curvature. Unfortunately, the swirling flows of interest in this study belong to this class. To investigate the extent of this problem, a simple swirling flow, that of the flow in a smooth annulus with the inner cylinder rotating, was considered.

Experimental data for this flow have been provided by Kuzay and Scott.[10] Sharma *et al.*[11] carried out a numerical study of the same flow. They were able to match the Kuzay–Scott data using a mixing length model that incorporated a modification suggested by Bradshaw.[10] An interesting feature of this flow is that the angular momentum is essentially constant across the fully turbulent core of the flow.

In terms of the k–ε model the modification suggested by Bradshaw[10] can be written as

$$\nu_t' = \nu_t(1-\beta Ri)^2, \tag{4}$$

where

$$Ri = \frac{k^2}{\varepsilon^2}\frac{W}{r^2}\frac{\partial}{\partial r}(rW). \tag{5}$$

The coefficient β is taken to be 5. The above modification is usually termed the Richardson number correction and was incorporated in FLOW3D using the user-defined routine USRVIS.

Calculations with and without the modification were carried out for various values of rotational speed of the inner cylinder.

Predicted curves of angular momentum are shown in Figure 3 for the standard model and for the case with the Richardson number correction. The Reynolds number is $2{\cdot}13 \times 10^5$ and the inner surface is rotating at a velocity equal to the mean axial velocity (62 m s^{-1}). It can be seen that the curve for the case with the correction displays the expected behaviour of a nearly constant value throughout, while the unmodified case does not.

Predictions of overall pressure drop per unit length are given in Figure 4 for the case of $\beta = 0$, i.e. with no Richardson number correction. The flow Reynolds number is $2{\cdot}13 \times 10^5$. For comparison, values estimated from Figure 7 of the paper by Sharma *et al.*[11] are included; the original data were not available. The predictions were used rather than the experimental data because Sharma *et al.*[11] showed that some of the flows measured by Kuzay and Scott[10] were not fully developed. It can be seen that the standard k–ε model consistently underpredicts the pressure drop. Also included is a prediction with the Richardson number correction included ($\beta = 5$). It can be seen that, for this one case at least, including the Richardson number correction significantly improves the pressure drop prediction.

The above results would appear to offer a simple method of improving the accuracy of the k–ε model within FLOW3D when applied to swirling flows. However, when the modification was applied to the case of flow over helical ribs, it was found that physically realistic, converged solutions were impossible to achieve. A converged solution could be achieved only if the correction was introduced gradually, i.e. if β was increased from 0 to 5 in small increments over several runs. However, the resulting solution was not physically realistic.

It must be concluded that while the Richardson number correction shows promise it improving the prediction of swirling flows, more work needs to be done on how to implement it within FLOW3D. It should be mentioned that no modifications were made to the wall functions. This is probably a major source of error, since most of the change of angular momentum occurs very

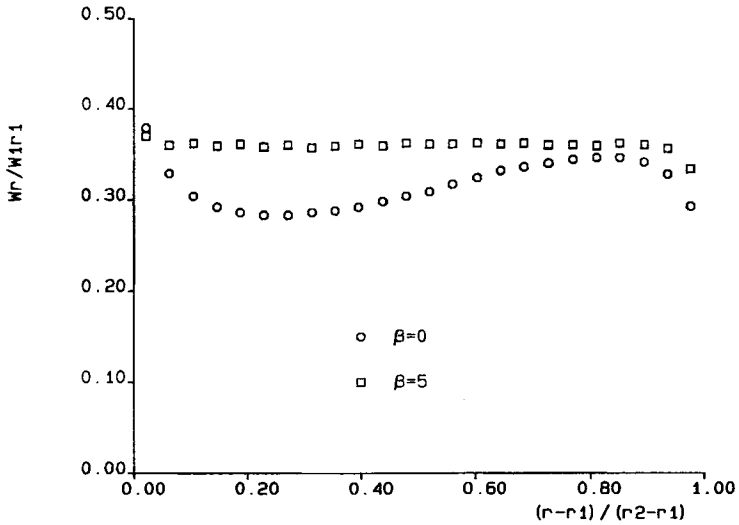

Figure 3. Predicted radial distribution of angular momentum in turbulent flow in a smooth annulus with inner cylinder rotating

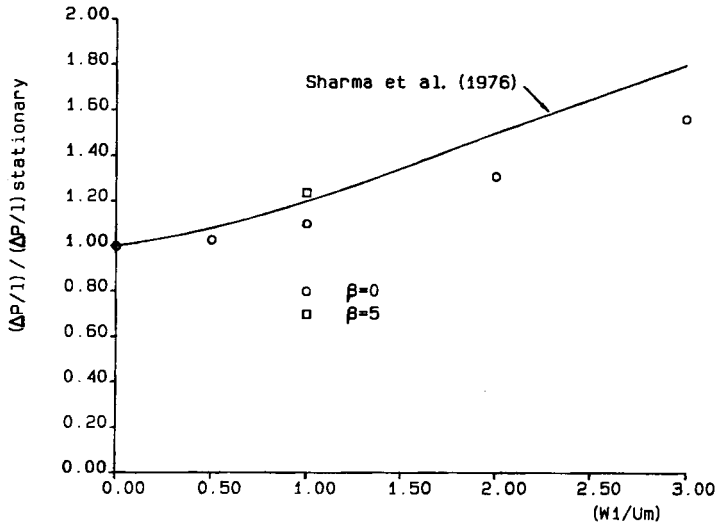

Figure 4. Predicted pressure drop for turbulent flow in a smooth annulus versus rotational speed of the inner cylinder

close to the wall. It would appear that the wall functions should be modified in such a way as to include the Richardson number effect. It is probably significant that Sharma *et al.*[11] did not use wall functions in their predictions, but solved to the wall. Unfortunately, modification of the wall functions within FLOW3D is not a straightforward exercise and time constraints did not permit further investigation of this matter.

The above calculations confirm the fact that the standard k–ε model is deficient in predicting swirling flows. Since it was not found possible to include the Richardson number correction to the calculation for flow over helical ribs, it must be expected that these deficiencies will manifest themselves in the results for these flows. For example, it can be expected that the predicted pressure drop will be lower than that found experimentally.

4.3. Flow over ribbed surfaces

Five rib geometries were considered: transverse ribs and 13°, 19°, 34° and 60° helical ribs. Velocity profiles for the 34° helical case are given in Figure 5. Included are the measurements of Pirie.[6] It can be seen that the model matches the angular velocity profile quite well, but the axial profile is less well predicted. The model predicts that the influence of the rib is only felt a few rib heights away from the roughened surface, but it is predicted to generate an average swirl velocity of approximately 20% of the axial component.

Near-wall values of the velocity components within the inter-rib channel are given in Figures 6–8. Figures 6 and 7 show evidence of separation and recirculation for the transverse case and the 13° helical case. Figure 8 again shows evidence that the 34° helical case generates the largest swirl velocity.

Near-wall values of kinetic energy, dissipation rate and eddy viscosity in the inter-rib channel are given in Figures 9–11 respectively. The relationship between viscosity, energy and dissipation assumed in the k–ε model requires that areas of relatively low energy and high dissipation are regions of low viscosity. This relationship is manifest in the three figures. Again, the non-dimensionalized viscosity can be interpreted as a turbulence Reynolds number and it can be seen that near the ribs the assumption of a high value of this parameter is violated.

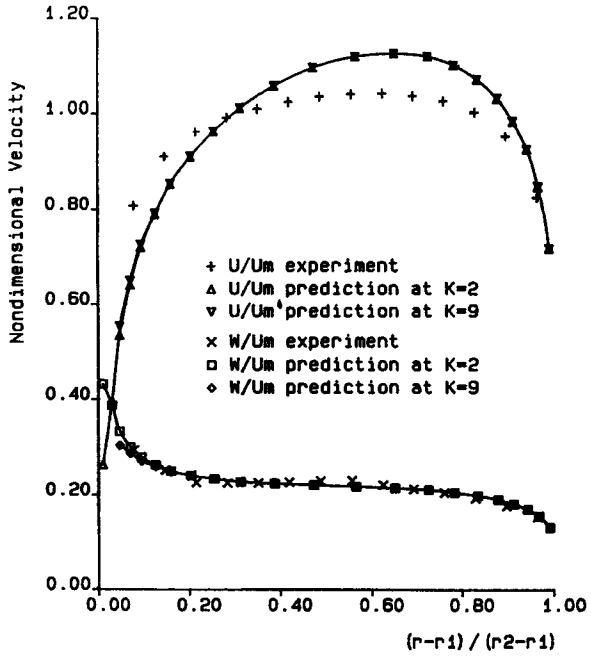

Figure 5. Predicted and experimental[6] velocity distributions for turbulent flow over 34° helical ribs (See Figure 2 for definition of K.)

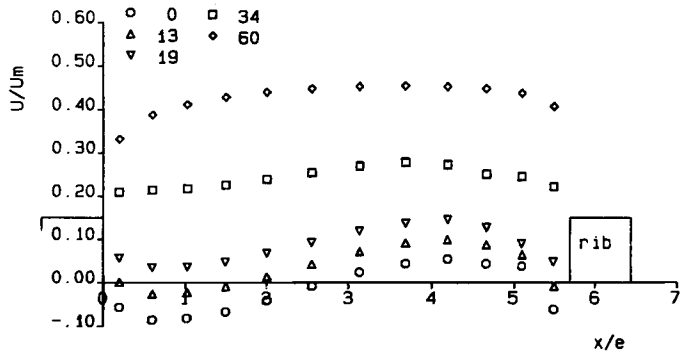

Figure 6. Predicted variation of near-wall $((r-r_1)/e=0{\cdot}25)$ axial velocities in the inter-rib channel of turbulent flow over transverse and helical ribs

Velocity vector plots are presented in Figures 12–16. These were constructed in order to investigate further the occurrence of separation and recirculation in the rib region. Only in the transverse rib case do the presented velocity vectors represent the total velocity. In all other cases the velocity vectors represent the components that lie in a radial–axial plane.

The transverse-ribbed case is shown in Figure 12 and it would appear that the flow separates upsteam and downstream of the rib. The upstream recirculation region is shown to be con-

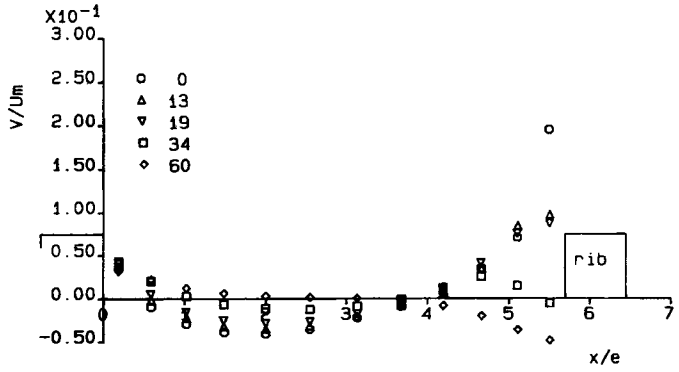

Figure 7. Predicted variation of near-wall ($(r-r_1)/e=0{\cdot}25$) radial velocities in the inter-rib channel of turbulent flow over transverse and helical ribs

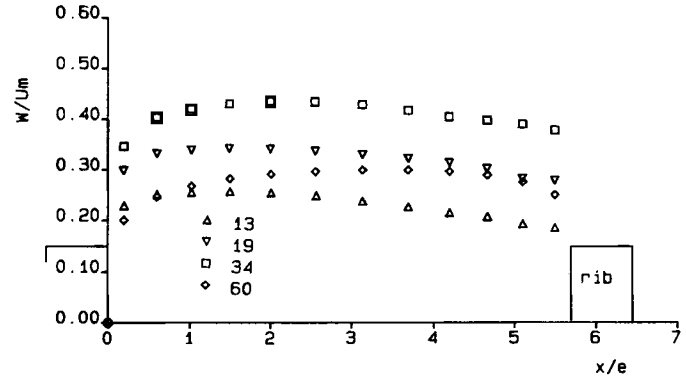

Figure 8. Predicted variation of near-wall ($(r-r_1)/e=0{\cdot}25$) angular velocities in the inter-rib channel of turbulent flow over helical ribs

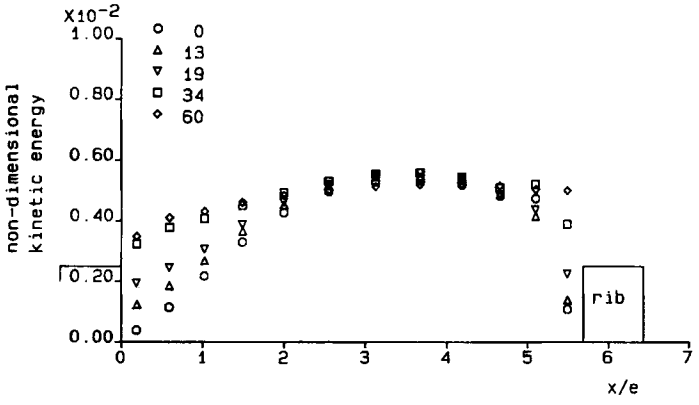

Figure 9. Predicted variation of near-wall ($(r-r_1)/e=0{\cdot}25$) dimensionless kinetic energy (k/U_m^2) in the inter-lab channel of turbulent flow over transverse and helical ribs

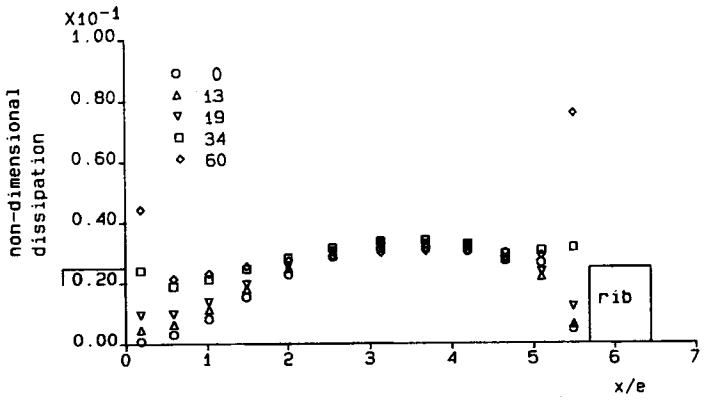

Figure 10. Predicted variation of near-wall $((r-r_1)/e=0{\cdot}25)$ dimensionless dissipation rate $(2(r_2-r_1)\varepsilon/U_m^3)$ in the inter-rib channel of turbulent flow over transverse and helical ribs

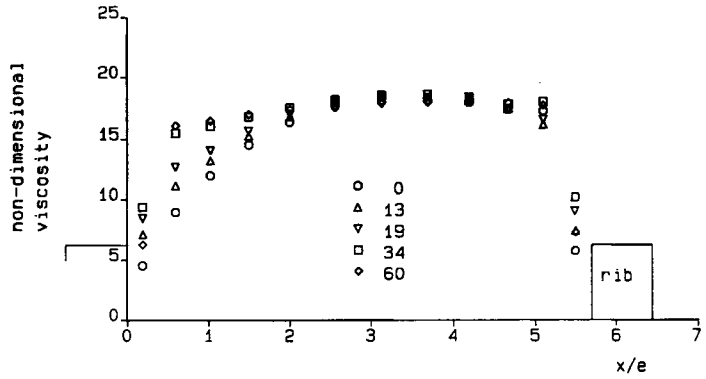

Figure 11. Predicted variation of near-wall $((r-r_1)/e=0{\cdot}25)$ dimensionless eddy (ν_t/ν) viscosity in the inter-rib channel of turbulent flow over transverse and helical ribs

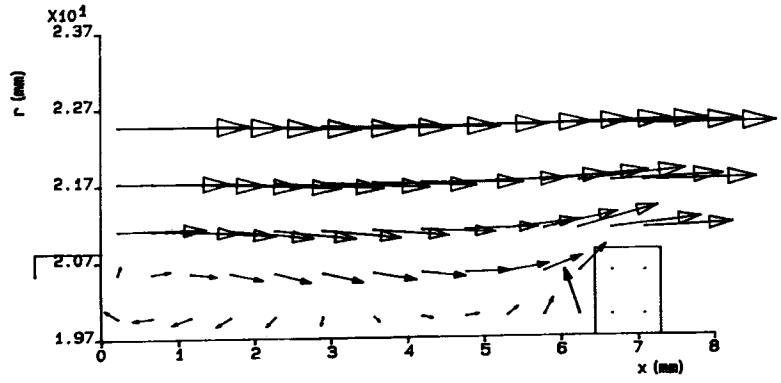

Figure 12. Predicted velocity vectors for turbulent flow over transverse-ribs

siderably smaller than the downstream region. These findings are compatible with the experimental data of Lawn[1] and the numerical predictions of Wilkes and Firth.[2]

The 13° helical-ribbed case is shown in Figure 13 to be similar to the transverse-ribbed case in that there is evidence of separation upstream and downstream of the rib. Separation in the 19° case, shown in Figure 14, would appear questionable. However, the plot could be interpreted as showing evidence of vortices tucked into the rib channel corners.

The 34° and 60° cases, shown in Figures 15 and 16 respectively, show no evidence of separtion. It must be remembered when considering the helical rib plots that the ribs are really at an angle to the paper and that the flow can appear to be going through the rib when in fact it is passing behind or in front of it. All five plots give further evidence of the fact that the rib influence is confined to a region only two to three rib heights high.

Values of axial and radial components of wall shear stress are presented in Figure 17. Only the transverse-ribbed and the 13° helical-ribbed cases show areas of negative axial shear. This supports the conclusion that probably only the 13° helical-ribbed case has areas of separation and recirculation either side of the rib. From Figure 17 it can be estimated that the reattachment point for the transverse case is predicted to be approximately 2·7 rib heights downstream of the rib's

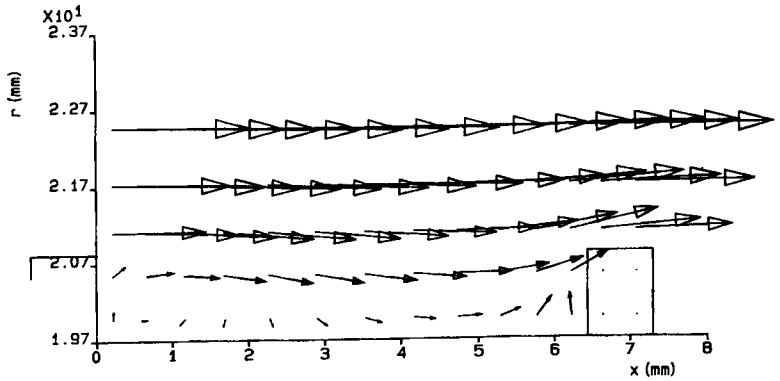

Figure 13. Predicted velocity vectors $(U+V)$ for turbulent flow over 13° helical ribs

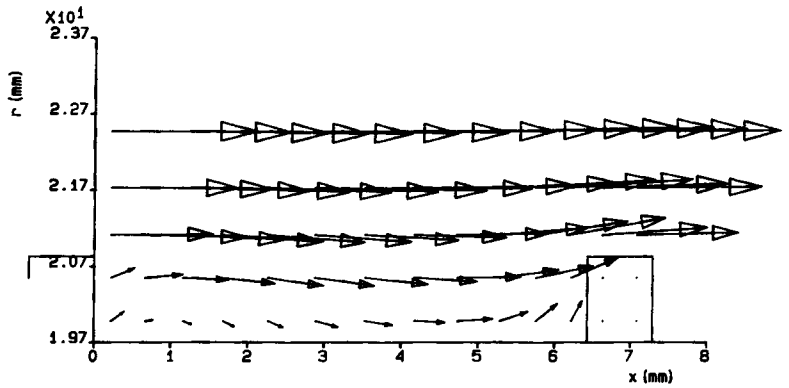

Figure 14. Predicted velocity vectors $(U+V)$ for turbulent flow over 19° helical ribs

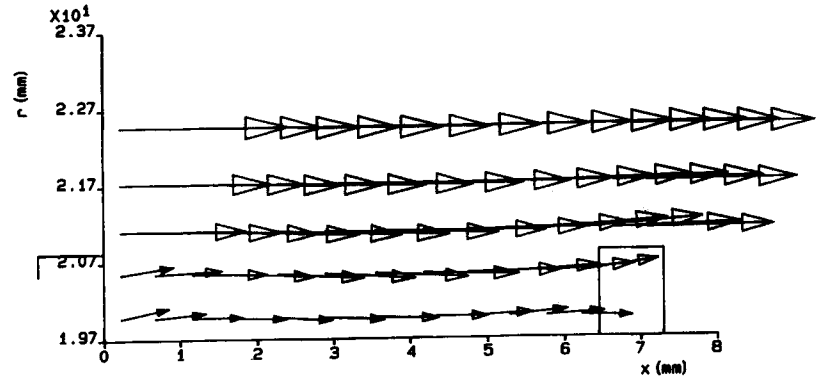

Figure 15. Predicted velocity vectors $(U+V)$ for turbulent flow over 34° helical ribs

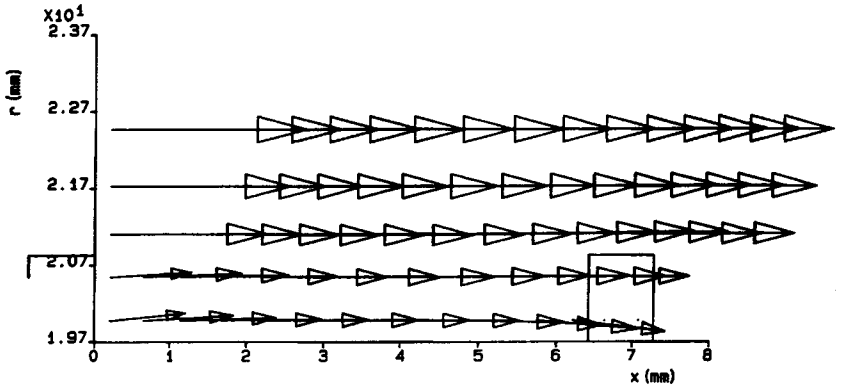

Figure 16. Predicted velocity vectors $(U+V)$ for turbulent flow over 60° helical ribs

back face. No experimental data appear to exist for the cylindrical transverse case nor for the helical cases, but Lawn's[1] data for the plane transverse case give a value of 2·3 rib heights. Corresponding angular components of wall shear are given in Figure 18 for the four helical-ribbed cases. It can be seen that the 34° case has the highest shear in the angular direction. This should be expected since it is this case that has the largest swirl velocity.

4.4. Pressure drop

Predicted axial variations of surface pressure for all cases are shown in Figure 19. As expected, the transverse-ribbed case is predicted to have the largest variation and largest overall pressure drop, and the 60° helical-ribbed case the least.

A curve of the predicted variation of overall pressure drop per unit length with rib angle for the turbulent cases is given in Figure 20. Pirie's[3] experimental data exhibit a similar trend to that seen in Figure 20. Pressure drop predictions for all cases considered are given in Table IV.

Included in Table IV is Pirie's[6] measured value for turbulent, flow over the 34° helical-ribbed case. It can be seen that the model predicts the pressure drop for this case to be approximately

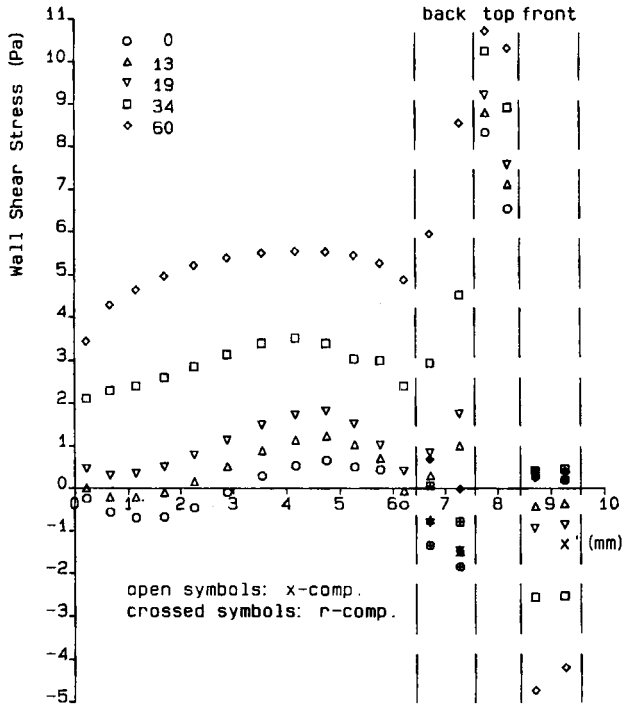

Figure 17. Predicted variation of axial and radial components of wall shear stress over the ribbed surface of turbulent flow over transverse and helical ribs

Table IV. Predicted and experimental[6] pressure drop per unit length

Case	$\Delta P/l$ (Pa m^{-1})
Transverse	1805
Helical	
13°	1685
19°	1542
34°	1139 (1682 exp.)
60°	753
Smooth	598

30% below the measured value. It is probable that the predicted pressure drop could have been improved by 'tuning' the constants in the model equations and/or those in the wall functions. However, no logical argument could be formed for doing so, particularly since the smooth-walled annuli pressure drop predictions were found to be accurate.

4.5. Grid refinement

The poor prediction of the axial velocity profile and overall pressure drop was thought to be due probably, in large part, to the coarseness of the grid employed. However, the values of near-

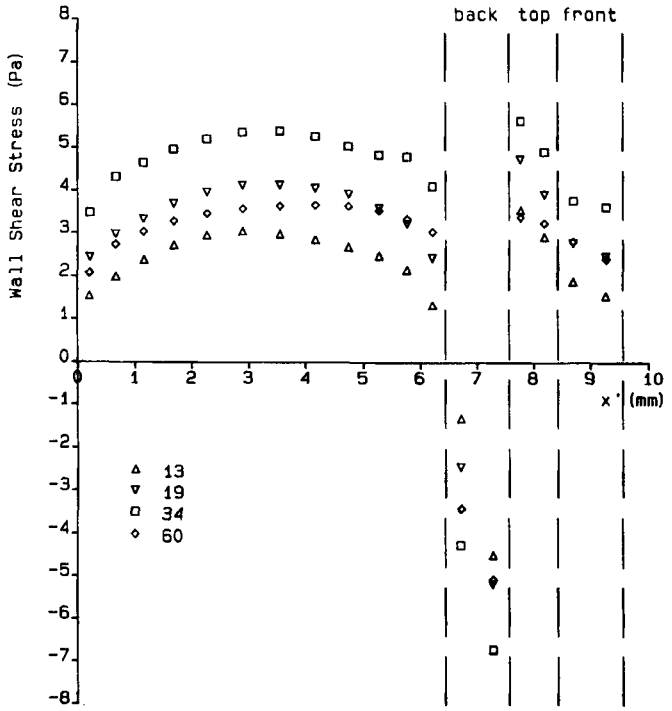

Figure 18. Predicted variation of angular component of wall shear stress over the ribbed surface of turbulent flow over and helical ribs

Table V. Refined grid details. *JV1* and *KV1* are the number of control volumes over the rib height and width respectively

Grid	*JV1*	*NJ*	*KV1*	*NK*
1	4	34	4	22
2	6	40	6	28
3	10	48	10	36

wall eddy viscosity presented in Section 4.3 indicated that often the near-wall points were at barely acceptable distances from the wall. It was shown in Section 4.1 that if grid refinement moved the near-wall points into the viscous sublayer, then it could be expected that the resulting prediction would be less accurate rather than more so. Hence any refinement at the design Reynolds number was not possible unless substantial changes were made to the turbulence model to account for molecular viscosity effects.

Grid refinement tests were carried out for the 34° helical rib case. In order to ensure that the near-wall points were above the viscous sublayer, the flow Reynolds number was raised to 10^6 by reducing the viscosity to $4{\cdot}182 \times 10^{-6}$. All other flow parameters remained the same as for the lower-Reynolds-number calculations. Three refined grids were used. Details are given in Table V.

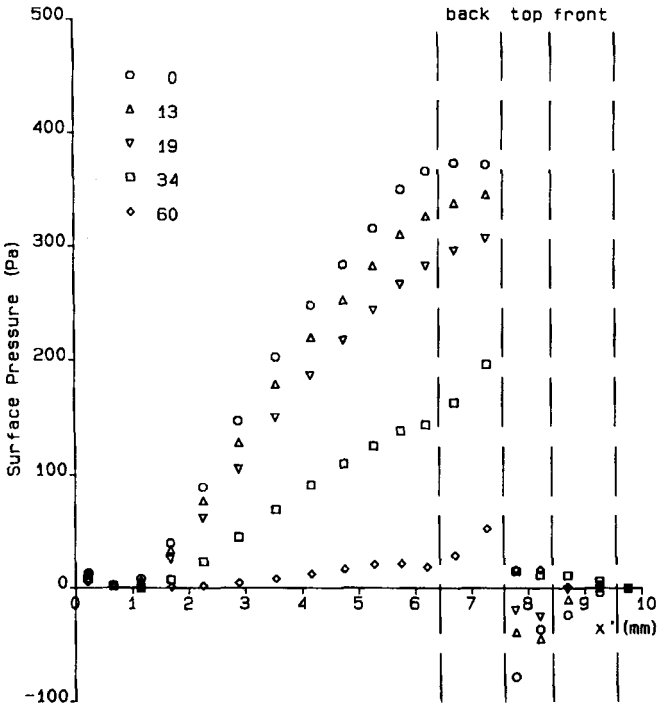

Figure 19. Predicted variation of pressure on the ribbed surface of turbulent flow over transverse and helical ribs

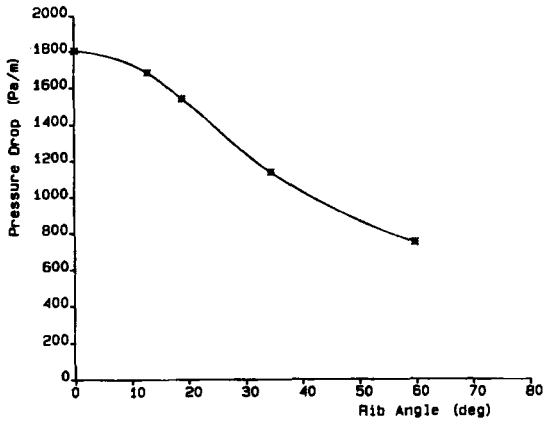

Figure 20. Predicted variation of pressure drop with rib angle

Axial velocity profiles for the coarse grid and for refined grid 3 are given in Figure 21. It can be seen that there is little difference between the coarse and refined grid profiles. The fact that predicted profile does not match the experimental curve would not appear to be a result of any inaccuracies introduced by the coarseness of the original grid.

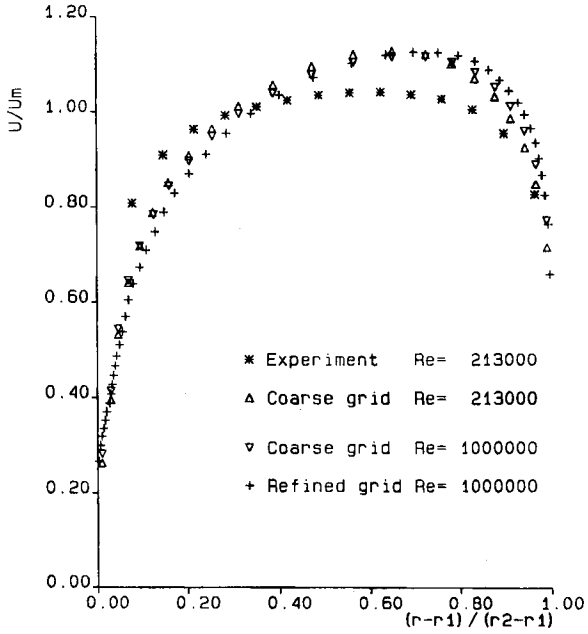

Figure 21. Coarse and refined grid predictions and measurements[6] of axial velocity distribution for turbulent flow over 34° helical ribs

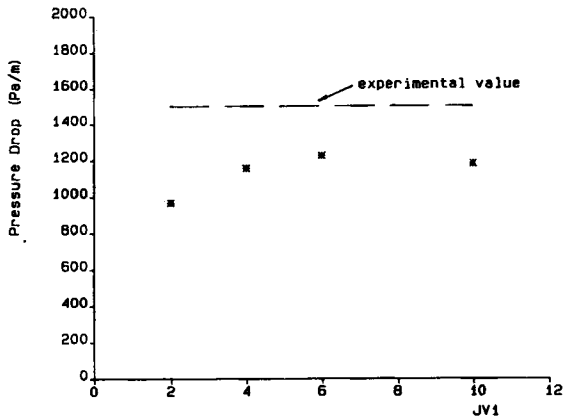

Figure 22. Influence of grid refinement on predicted pressured drop for turbulent flow over 34° helical ribs. Experimental value due to Pirie[6]

The predicted overall pressure drop per unit length as a function of the number of control volumes used to resolve the rib height is given in Figure 22. The actual predicted values are given in Table VI together with minimum y^+-values. It can be seen that grid refinement increased the predicted pressure drop by almost 27%. However, even the largest refined grid pressure drop prediction is approximately 18% lower than that estimated from Pirie's[6] experiments. The fact that refined grid 3 gave a slightly lower value than refined grid 2 may be due to the fact that some of the near-wall points of the more refined grid were too close to the viscous sublayer.

Table VI. Grid refinement results ($Re = 10^6$)

Grid	$\Delta P/l$ (Pa m^{-1})	y^+_{min}
Coarse	968	84
Refined		
1	1157	42
2	1226	26
3	1187	12
	1500	(exp.)

A further reason for carrying out the grid refinement exercise was to investigate the possibility that the original grid used was too coarse to pick up any separation of the flow about the ribs. However, the refined calculations showed no evidence of separation and generally confirmed the trends predicted using the coarse grid.

While grid refinement has been shown to improve the pressure drop prediction, it would seen obvious that there are other factors contributing to the poor pressure drop and axial velocity profile predictions. It is more than likely that these factors have their roots in the underlying assumptions used in the construction of the standard k–ε turbulence model; in particular, the neglect of the effect of streamline curvature.

5. CONCLUSIONS

Turbulent flow through annuli with rib-roughened inner cylinders has been modelled using FLOW3D. Where possible the results have been compared with existing data. It has been predicted that there are significant differences between turbulent flow over helical-ribbed cylinders compared to that over cylinders with transverse ribs. It is difficult to dismiss these differences as simply due to any lack of precision in the results. This is because all predictions are of comparable accuracy and the predictions for the transverse case agree in general with the measurements of Lawn[1] and the predictions of Wilkes and Firth.[2] However, grid refinement did produce improvements in overall pressure drop.

It was predicted that there are no regions of separation and recirculation in turbulent flow over the helical-ribbed geometry except for very acute rib angles; specifically, less than 19°. The results show that the flow travels more smoothly over helical-ribbed cylinders and this would seem to be the mechanism responsible for the reduction in pressure drop. Also, the substantial increase in the magnitude of the near-wall velocities in the inter-rib channel of the helical-ribbed cylinder compared to the transverse-ribbed case would suggest that 'hot spots' are less likely to occur in the former case.

The differences seen between the experimental data and the predictions for turbulent flow over the rib-roughened surfaces underline the need for improvement in the k–ε turbulence model. The Richardson number correction showed some promise, but more work needs to be done in implementing it within FLOW3D. It also appears that the use of wall functions for the ribbed geometry considered may not be appreciate. However, solving to the wall would require a radial modification to the model equations within FLOW3D.

ACKNOWLEDGEMENTS

This work was supported by a Central Electricity Generating Board Contract No. RK 1679. The authors would also like to thank Mr. H. G. Lyall, Drs. S. A. Fairbairn, R. J. Firth, R. T. Szczepura

and Mr. M. A. M. Pirie at Berkeley Nuclear Laboratories and Drs I. P. Jones and N. S. Wilkes and their colleagues at AERE Harwell for many helpful discussions.

APPENDIX: NOTATION

C	a constant
D	diameter
e	rib height
f	friction factor
JV	number of control volumes across smooth channel
$JV1$	number of control volumes across rib height
k	turbulence kinetic energy
l	axial distance
NJ	total number of control volumes in J-direction
NK	total number of control volumes in K-direction
P	time-averaged pressure
P^*	pseudo-pressure
Re	Reynolds number ($Re=\rho(D_2-D_1)U_m/\mu$)
Re_t	turbulence Reynolds number
r	radical position
U_m	bulk or mean velocity
u^*	$(\tau_w/\rho)^{1/2}$
W	velocity in angular direction
x	axial position
y	normal distance from solid wall
y^+	yu^*/ν
β	a constant
ΔP	pressure drop
ε	rate of energy dissipation
μ	viscosity
ν	kinematic viscosity
ν_t	kinematic eddy viscosity
ν_t'	see equation (4)
ρ	density
τ_w	wall shear stress

REFERENCES

1. C. J. Lawn, 'Flow measurements for establishing the mechanism of heat transfer from rib-roughened surfaces', *CEGB Report RD/B/N3514*, 1976.
2. N. S. Wilkes and R. J. Firth, 'Prediction of fluid flow over a transverse-ribbed surface using finite difference methods with a $k-\varepsilon$ turbulence model', *CEGB Report RD/B/5098N81*, 1981.
3. M. A. M. Pirie, 'Heat transfer and pressure drop tests on multi-start ribbed surfaces covering the rib angle range zero to sixty degrees', *CEGB Report RD/B/N2760*, 1974.
4. A. D. Burns, I. P. Jones, J. R. Kightley and N. S. Wilkes, 'The implementation of a finite difference method for predicting incompressible flows in complex geometries', *Proc. Numerical Methods in Laminar and Turbulent Flows*, Pineridge, Swansea, 1987, p. 339.
5. I. P. Jones, J. R. Kightley, C. P. Thompson and N. S. Wilkes, 'FLOW3D, a computer code for the prediction of laminar and turbulent flow and heat transfer: release 1', *UKAEA Report AERE-R 11825*, 1985.
6. M. A. M. Pirie, CEGB, BNL, *Personal communication*, 1989.

7. C. J. Lawn and C. J. Elliot, 'Fully developed flow through concentric annuli', *CEGB Report RD/B/N1878*, 1971.
8. F. S. Henry and A. J. Reynolds, 'An analytical solution to two gradient diffusion models of turbulence', *J. Fluids Eng.*, **106**, 211–216 (1984).
9. P. Bradshaw, 'The analogy between streamline curvature and buoyancy in turbulent shear flow', *J. Fluid Mech.*, **36**, 177–191 (1969).
10. T. M. Kuzay and C. J. Scott, 'Turbulent heat and momentum transfer studies in an annulus with rotating inner cylinder', *University of Minnesota, Heat Transfer Laboratory, TD No. 111*, 1973.
11. B. I. Sharma, B. E. Launder and C. J. Scott, 'Computation of annular, turbulent flow with rotating core tube', *J. Fluids Eng.*, **98**, 753–758 (1976).